Implications of a non-linear $^{40}Ar/^{39}Ar$ age progression along the Louisville seamount trail for models of fixed and moving hotspots

Anthony A.P. Koppers[1*], Robert A. Duncan[2] and Bernhard Steinberger[3]

[1] Institute of Geophysics and Planetary Physics
Scripps Institution of Oceanography
University of California, San Diego
La Jolla, CA 92093-0225, USA
[2] College of Oceanic & Atmospheric Sciences
Oregon State University
104 Ocean Administration Building
Corvallis, OR 97331-5503, USA
[3] IFREE, JAMSTEC
2-15 Natsushima-cho
Yokosuka-shi
Kanagawa 237-0061, Japan
[*] Corresponding Author: akoppers@ucsd.edu; +1 858 534 8090 (fax)

First Submission
G3
Research Letter
December 3, 2003

word count = 6198

abstract

The Louisville seamount trail has been recognized as one of the key examples of hotspot volcanism — next to the classic volcanic Hawaiian-Emperor lineaments. Although little data have become available over the last decades for this seamount trail, the published total fusion $^{40}Ar/^{39}Ar$ data of Watts et al. (1988) showed an astonishing linear age progression, firmly establishing Louisville as a ***fixed*** hotspot in the South Pacific mantle. We report new $^{40}Ar/^{39}Ar$ ages based on high-resolution incremental heating $^{40}Ar/^{39}Ar$ dating for the same group of samples, showing a marked increase in both precision and accuracy. One of the key findings in our re-examination is that the age progression is ***not*** linear after all. The new data show a significantly decreased "apparent" plate velocity for the Louisville seamount trail older than 62 Ma, but confirm the linear trend between 47 Ma and the present day (although only based on 3 samples over 2,150 km). The most recent volcanic activity at the Louisville seamount trail has now been dated at 1.11 ± 0.04 Ma for the most southeastern seamount located at 50º26'S and 139º09'W. These results indicate that the Louisville age progression should be interpreted on basis of both plate and hotspot motion. In this paper, we examine our new results in conjunction with the numerical mantle flow models of Steinberger et al. (2003) that also predict marked deviations from simple linear age progressions. With these models we can

achieve a good fit to the geometry of both the Hawaiian and Louisville seamount trails and their age progressions, as well as the ~15º paleo-latidunal shift observed by Tarduno et al. (2003) for the Hawaiian hotspot between 80 and 47 Ma. Improved mantle flow models, including Pacific hotspots only, show that we can also fit the non-linear age trend for the Louisville seamount trail by allowing an additional rotation of the Pacific plate around 62 Ma and by decreasing the initiation age of the Louisville hotspot from 120 to 90 Ma. This improved model requires a significant eastward hotspot motion of ~7º between the 80 and 40 Ma for the Louisville hotspot, which is quite dissimilar to the southward motion of the Hawaiian hotspot during the same time interval, followed by a minor ~2º latitudinal shift over the last 40 Myr. If hotspot tracks are considered globally, the age trend observed for the oldest part of the Louisville seamount trail does not entirely follow the numerical model predictions. This may indicate some remaining inaccuracies in the global plate circuit, but it may also indicate that the Louisville hotspot experienced a motion somewhat different than in the numerical model — faster in the interval between 62 and 47 Ma, but slower before that.

Keywords $^{40}Ar/^{39}Ar$ geochronology; seamounts; guyots; submarine alteration; Pacific plate; hotspots; intra-plate volcanism; mantle flow models; inter-hotspot motion

1. Introduction

The Louisville seamount trail (Figure 1) is a 4,300 km long chain of submarine volcanoes that are inferred to have been built in the past 80 Myr as the Pacific plate moved over a persistent melt anomaly or hotspot (Hawkins *et al.* 1987; Lonsdale 1988). The Louisville hotspot is considered the South Pacific counterpart of the much better studied Hawaiian hotspot and represents one of only three primary hotspots in the Pacific basin (Courtillot *et al.* 2003). Recent ocean drilling in the Emperors Seamounts, followed by paleomagnetic analyses of cored samples, has documented a substantial ~15° southward motion of the Hawaiian hotspot prior to 47 Ma (Tarduno *et al.* 2003) and, as a result, calls into question whether Pacific hotspots constitute a fixed reference frame in the Earth's deep mantle. One end member model advocates that the primary hotspots moved in concert and would comprise a relatively fixed or slowly moving reference frame (Courtillot *et al.* 2003). Another model, based on numerical mantle flow modeling and seismic tomography, reproduces the observed latitudinal motion for the Hawaiian hotspot, but predicts essentially no latitudinal motion for the Louisville hotspot (Steinberger *et al.* 2003). Even other models would abandon the mantle plume hypothesis altogether, explaining the Louisville seamount trail by (thermal) extension in the Pacific lithosphere or a genetic relation with the Eltanin fracture zone (Smith and Lewis 1999; Foulger and Natland 2003).

The paleolatitude data and $^{40}Ar/^{39}Ar$ age systematics of seamount trails provide us with the only data to directly test these models. Where the paleolatitude data give us a location record of the volcanic source (or hotspot) over

geological time and relative to the geocentric dipole, the age progressions are the sum of both plate and hotspot motions. It has been shown previously by Koppers et al. (2001) that $^{40}Ar/^{39}Ar$ age progressions along seamount trails are in most cases ***inconsistent*** with the fixed hotspot hypothesis, allowing for possible inter-hotspot motions up to 60 mm/yr. The differences in the observed age progressions thus are significant and allow us to distinguish between models of fixed and moving hotspots. It follows, therefore, that defining the $^{40}Ar/^{39}Ar$ age progressions along seamount trails both accurately and precisely is critical to assessing hotspot and other models for intra-plate volcanism (see review by Koppers *et al.* 2003b).

Watts et al. (1988) reported total fusion $^{40}Ar/^{39}Ar$ ages from nine seamounts that span the entire length of the Louisville seamount trail and that produced a surprisingly linear age progression (Figure 2). Since that time $^{40}Ar/^{39}Ar$ techniques have significantly improved by instrumental developments, better sample preparation methods and more rigorous applications of the incremental heating technique. Submarine basalts can now be dated more accurately, because internal tests can be performed to identify samples that have been adversely affected by submarine alteration (Koppers *et al.* 2000; Koppers *et al.* 2003b). This clearly makes the conventional K-Ar and total fusion $^{40}Ar/^{39}Ar$ techniques unsuitable for dating altered seamount basalts since both fall short in discriminating between fresh and altered seamount basalts, and those affected by excess (mantle-derived) argon (cf. McDougall and Harrison 1988).

We have re-dated 10 samples from the Watts et al. (1988) study by applying high-resolution $^{40}Ar/^{39}Ar$ incremental heating experiments (Figure 3; Table 1 & 2) that significantly improved the accuracy of the age determinations for the Louisville seamount trail. It is evident that samples older than 62 Ma have incremental heating $^{40}Ar/^{39}Ar$ ages that are older than the previous ages determined by the total fusion technique (Table 3). A simple explanation is that these samples are too altered to provide reliable (total fusion) crystallization ages due to both radiogenic ^{40}Ar and $^{39}Ar_k$ loss, but that the incremental heating experiments were able to resolve these secondary processes and provide reliable age plateaus and isochrons. Our new results show that the age progression for the Louisville seamount trail is ***not*** linear after all, but requires another interpretation of the $^{40}Ar/^{39}Ar$ ages in the light of the current paradigm of fixed versus moving hotspots.

In this paper, we present new high-resolution $^{40}Ar/^{39}Ar$ data for the Louisville seamount trail and discuss the systematics of groundmass dating for altered seamount basalts (cf. Koppers *et al.* 2000). We also discuss the impact of the resulting non-linear age progression on the important question of hotspot fixity and make comparisons with the new age systematics of the Hawaiian-Emperor seamount trail (Sharp and Clague 2002; Tarduno *et al.* 2003). Finally, we present new results of mantle flow models that offer a possible explanation for

the observed age systematics in both the Louisville and Hawaiian hotspot trails.

2. $^{40}Ar/^{39}Ar$ Dating Techniques

In total we dated 13 samples using the $^{40}Ar/^{39}Ar$ incremental heating technique from 10 seamounts or guyots in the Louisville seamount trail. This sample set contains two samples (SOTW-9-58-7 and VM36-02) that were not dated by Watts et al. (1988). The results of these incremental heating experiments are displayed in age plateau and isochron diagrams in Figure 3; the corresponding isotopic data are listed in Table 2. Analytical data can be downloaded from the EarthRef.org Digital Archive (ERDA) as detailed in Appendix A.

The incremental heating $^{40}Ar/^{39}Ar$ age determinations were performed on crystalline groundmass separates (250-500 μm) and one plagioclase mineral separate (250-500 μm) using a continuous, 10W CO_2 laserprobe combined with a MAP-215/50 mass spectrometer at Oregon State University. Sample preparation and acid leaching are described in Koppers et al. (2000). The mass spectrometer is a 90° sector instrument with a Nier-type source with an all-metal extraction system for $^{40}Ar/^{39}Ar$ age determinations. It has an electron multiplier for high sensitivity and an electrostatic analyzer with adjustable collector slit for an effective resolution (~600) of Ar peaks from small hydrocarbon peaks. Irradiated groundmass samples were loaded into Cu-planchettes designed with a variety of pans that hold up to 50 mg of material, which are then pumped within a sample chamber fitted with a ZnSe window transparent to the CO_2 laser wavelength. Software allows for scanning across samples in a preset pattern with a defocused beam, to evenly heat the material. Gas cleanup was accomplished with a series of Zr-Al getters. All argon ages were measured relative to the flux monitor standard FCT-3 biotite (28.04 ± 0.18 Ma, 1σ, Renne *et al.* 1994) and calculated using the corrected Steiger and Jäger (1977) decay constant of 5.530 ± 0.097 x 10^{-10} 1/yr (2σ) as reported by Min et al. (2000). For a detailed description of the analytical facility and the constants used in the age calculations we refer to Table 2 in Koppers et al. (2003a). Incremental heating plateau ages and isochron ages were calculated as weighted means with $1/\sigma^2$ as weighting factor (Taylor 1997) and as YORK2 least-square fits with correlated errors (York 1969) using the ArArCALC v2.2 software from Koppers (2002) that is available from the http://earthref.org/tools/ararcalc.htm website. In this paper, all errors on the $^{40}Ar/^{39}Ar$ ages are reported at the 95% confidence level (2σ), unless otherwise indicated.

3. Results and Discussion

In this section, we interpret the $^{40}Ar/^{39}Ar$ age spectra (Figure 3, 4 and 5) and assess the quality of the groundmass incremental heating experiments. In this section, we interpret the $^{40}Ar/^{39}Ar$ age spectra (Figure 3, 4 and 5) and assess the quality of the groundmass incremental heating experiments. We discuss our new age results for the Louisville seamount trail in the context of various hotspot models, while addressing the non-linear character of the observed age progression and its inferences for the motion of the Louisville hotspot. We finish by comparing the $^{40}Ar/^{39}Ar$ age progressions for the Louisville and Hawaiian-Emperor seamount trails, and by using these data sets to calibrate and test new mantle flow models for the Pacific mantle.

3.1. $^{40}Ar/^{39}Ar$ geochronology of seamount basalts

Although $^{40}Ar/^{39}Ar$ dating of seamount basalts by mineral separates (plagioclase, hornblende, biotite) in most cases is preferable over whole rocks due to their more homogenous degassing behavior, in reality, we are limited by a lack of suitable phenocrystic materials in dredge collections. Out of a necessity, dating basaltic groundmass samples using $^{40}Ar/^{39}Ar$ incremental heating techniques has become a powerful tool when studying the evolution of seamount trails (Koppers *et al.* 1998; 2003b). It has been shown that crystalline groundmass samples provide ages concordant with $^{40}Ar/^{39}Ar$ ages of co-magmatic minerals and, therefore, can be interpreted as eruption ages (Koppers *et al.* 2000). In this study, we have applied the same groundmass dating technique to date the Louisville seamount basalts that are mildly alkalic with molar K/Ca ratios ranging from 0.05 to 0.38. Our high-resolution incremental heating experiments comprised 16-30 individual heating steps, allowing us to better resolve primary $^{40}Ar/^{39}Ar$ age signals from alteration and irradiation-induced disturbances. The resulting age spectra are well-defined with wide age plateaus (50-75% of the total gas released) that comprise between 7 and 16 individual heating steps. The isotopic compositions for these age plateau steps generally show a reasonable dispersion in their radiogenic ^{40}Ar component and result in isochrons (Koppers *et al.* 2000; Kuiper 2002) with calculated $^{40}Ar/^{36}Ar$ intercept values indistinguishable from the 295.5 atmospheric ratio, ruling out excess ^{40}Ar. It is noteworthy that most of the "final melting points" fall on the reference line between the atmospheric intercept on the $^{36}Ar/^{40}Ar$ axis and the argon age intercept on the $^{39}Ar/^{40}Ar$ axis (Figure 3). This indicates that the trapped argon in the groundmass samples has an initial $^{40}Ar/^{36}Ar$ ratio close to the 295.5 value in modern air. Finally, the total fusion points also fall close to or on these reference lines (see the orange circles in Figure 3) indicating that the isochron, plateau and total fusion ages are concordant at the 2σ confidence level. These observations are all good indicators for the high quality of the $^{40}Ar/^{39}Ar$ groundmass ages on these seamount basalt samples.

The groundmass argon release patterns thus prove to be characteristic (Figure 3 and 4) and allow us to explain the degassing behavior of (holo-)crystalline groundmass samples during incremental heating experiments (Figure 5). The low temperature (LT) increments typically are characterized by high apparent ages, high K/Ca ratios and significant spikes in the $^{36}Ar_{atm}$ and $^{38}Ar_{cl}$ components that reflect high contributions in the total argon inventory from atmospheric components and chlorine. All these observations can be explained by the recoil of $^{39}Ar_K$ (high apparent ages) as associated with the preferential degassing of fine-grained alteration phases (high K/Ca ratios; spikes in both the $^{36}Ar_{atm}$ and $^{38}Ar_{cl}$ components) that remain in the groundmasses, even though the samples were treated by intensive acid-leaching (Koppers *et al.* 2000). Electron microprobe analyses have shown that this remaining alteration is most likely located interstitially and on the surfaces of groundmass minerals, which can be effectively removed by applying extended heating schedules (Koppers *et al.* 2000). In the isochron diagrams, the discordant LT steps start off from the atmospheric intercept on the $^{36}Ar/^{40}Ar$ axis, followed by a curved approach towards the isochron, as shown by the light blue arrows in Figure 3. These concave curves are best explained by the degassing of predominantly alteration phases at the lowest temperatures (light blue circles) and an increasing contribution of primary groundmass degassing (red circles) with higher temperatures, generating sub-horizontal mixing lines in the isochron diagrams. During this degassing stage the atmospheric component is continuously diminishing (Figure 4) until the released argon gasses for individual heating steps are about 80-100% radiogenic. This process causes a decreasing $^{36}Ar/^{40}Ar$ trend in isochron diagrams. In reality, all three processes start to act together almost immediately following the onset of the incremental heating, resulting in a more "curved" array of data points, as is usually observed in the isochron diagrams (Figure 3).

Well-resolved age plateaus develop at the intermediate temperature steps that are high in their radiogenic ^{40}Ar component (80-100%) and that show almost no contribution from the $^{38}Ar_{cl}$ component (Figure 4). We conclude, therefore, that the effects of alteration and $^{39}Ar_K$ recoil are negligible, at least, within these experiments. Their age plateaus may still reveal subtle systematic changes (such as declining or arching upward age profiles) that can be attributed to the remaining effects of recoil and alteration on the age spectra. However, their contribution is minor, in particular, since the calculated MSWD values never exceed 5.3 (Table 2) and since the disturbances all occur within the 95% confidence envelope. The plateau ages thus represent well-defined crystallization ages, as is confirmed by the fact that most plateau ages are consistent with their isochron and total fusion ages, and that $^{40}Ar/^{36}Ar$ intercept values are indistinguishable from the 295.5 atmospheric ratio. It is important to note here that in the inverse isochron diagrams the data points representing the age plateaus form clear arrays running parallel to the reference line between the plateau age on the $^{39}Ar/^{40}Ar$ axis and the 295.5 atmospheric intercept on

the $^{36}Ar/^{40}Ar$ axis (Figure 3 and 5). These arrays form distinct linear segments with different angles compared to the discordant low and high temperature data points, which indicates that the age plateaus are not (significantly) affected by the same secondary (alteration) processes and disturbances. Instead, they represent bi-modal mixing lines between the radiogenic and atmospheric components.

The high temperature (HT) steps are characterized by minor (but significant) decreases in their apparent age, strong decreases in the K/Ca ratios and large increases in the $^{37}Ar_{Ca}$ and $^{36}Ar_{atm}$ components (Figure 4) that reflect the preferential degassing of clinopyroxene and plagioclase minerals. In some cases a second increase is observed for the $^{38}Ar_{cl}$ component (Figure 4) that might be related to primary chlorine contents of clinopyroxene and plagioclase in the crystalline groundmass samples. These discordant HT steps show a clear departure from the isochrons, as is indicated by the light orange arrows in Figure 3. These convex curves first move towards higher $^{39}Ar/^{40}Ar$ ratios and then quickly towards the atmospheric intercept for the final heating steps, where they may intersect with the isochron reference line, indicating that the trapped argon in these samples is atmospheric and thus does not contain significant excess argon. The low apparent ages can be explained by the recoil loss of irradiation-produced $^{37}Ar_{Ca}$ or the diffusion of $^{39}Ar_K$ into the HT clinopyroxene and plagioclase phases following recoil from the LT high potassium (alteration) phases.

We have shown that dating crystalline groundmass samples provide $^{40}Ar/^{39}Ar$ ages that are reliable estimates of the crystallization ages of seamount basalts, in particular, in absence of suitable potassium-bearing minerals to be dated. These improved ages paint a different picture in terms of the age progression along the Louisville seamount trail, when compared to the original Watts et al. (1988) study, and have important consequences for the fixed hotspot model.

3.2. Analyses of the non-linear age progression

We have redated most samples from the Watts et al. (1988) except those that were judged too glassy or too much altered. We were able to add two new age determinations for samples SOTW-9-58-7 and VM36-02 that were dredged from Osbourn Seamount in the northwestern segment and an unnamed seamount in the middle segment of the Louisville seamount trail (Figure 1). Based on improved methodology, we significantly increased both the accuracy and precision (10-89% improvements) when compared to the total fusion ages of the Watts et al. (1988) study (Table 3). The new ages are 11-12 Myr (16%) older in the oldest part of the Louisville seamount trail. This clearly indicates a significant change in "apparent" plate *vs.* hotspot velocity for the Pacific plate prior to 62 Ma when compared to previous studies on plate motion (e.g. Duncan and Clague 1985; Lonsdale 1988;

Wessel and Kroenke 1997; Koppers *et al.* 2001). Samples younger than 62 Myr are more compatible with the previous total fusion ages, confirming the linear trend between 47 Ma and the present day (although based only on 3 samples over 2,150 km). We were also able to date the most recent volcanic activity at the Louisville seamount trail at 1.11 ± 0.04 Ma for the most southeastern seamount at 50º26'S, 139º09'W.

The new incremental heating ages thus show a non-linear age progression indicated by the orange dashed line in Figure 2 that follows the oldest observed ages along this seamount trail. This line includes only the high-resolution incremental heating ages from this study; it does, however, not include a re-analysis of the ~55 Ma total fusion age for sample VM-36-05 that is located 3,100 km from the present day Louisville hotspot, because this sample contains too much volcanic glass to be useful for $^{40}Ar/^{39}Ar$ dating. An alternate age progression is shown by the purple dotted line as based on mantle convection models of Steinberger et al. (2003). Their models allow for the movement of the Louisville hotspot over geological time, which is reflected in a different age-distance relationship that is consistent with the older ages for Osbourn seamount, but not with the general age trend at the older end of the seamount trail. Adjusted models show a better agreement, as discussed in the next paragraph.

3.3. Evaluating mantle flow models allowing for hotspot motion

We now evaluate whether the motion of hotspots derived from current models of mantle flow, in combination with various plate rotation models, are adequate to explain the geometries and age progressions of the Hawaiian and Louisville seamount trails, and for which model parameters we find the best fit to the highest quality age data, including the new $^{40}Ar/^{39}Ar$ ages reported in this paper. These models have been previously described in more detail (e.g. Steinberger and O'Connell 1998; Steinberger 2000) and include two steps. In the first step, a large-scale mantle flow field is computed based on internal density heterogeneities as inferred from seismic tomography studies, the viscosity structure of the mantle and plate motions. In the second step, a plume conduit is inserted into this flow field that is assumed to rise vertically in the beginning, but which is subsequently advected into the large-scale mantle flow while rising buoyantly. The conduit source or root is assumed to move with the horizontal flow component at its source depth in the lowermost mantle. In this discussion, we will use the same modeling assumptions as in the "moving source models" of Steinberger et al. (2003) and Tarduno et al. (2003), except where specifically noted. We will begin this discussion by considering the Hawaiian and Louisville hotspots as part of the Pacific convection system only, but we will conclude with models that attempt to optimize the global fit to all hotspot tracks and the global plate circuit, in a similar approach as Steinberger et al. (2003). All tracks shown are computed for Pacific plate motion with no boundary or intra-plate deformation

between the North and South Pacific

The brown lines in Figure 6 show the best-fitting tracks (left panels) and age progressions (right panels) for the Steinberger et al. (2003) model of Hawaiian and Louisville hotspot motion (Case 1). In this moving hotspot model four stages of constant Pacific plate rotation are allowed, with a major plate motion change at 47 Ma that marks the revised age of the bend in the Hawaiian-Emperor seamount trail (Sharp and Clague, 2002). Another change in plate motion around 62 Ma permits an improved fit to the age progression of the older part of the Louisville seamount trail, as new high-resolution $^{40}Ar/^{39}Ar$ ages indicate a slower plate motion prior to 62 Ma. Furthermore, the fit to the geometry and age data of the 0-47 Ma part of both tracks is considerably improved, if an additional change in plate motion is allowed at 25 Ma (cf. Koppers *et al.* 2001). While the overall fit of the Steinberger et al. (2003) model is very good, the computed ages for the older part (> 47 Ma) of the Hawaiian track tend to be up to 3 Myr younger and for the corresponding part of the Louisville track up to 5 Myr older.

We find that this model can be further improved, if we assume a plume initiation age for the Louisville hotspot of 90 Ma instead of 120 Ma (Case 2). Recent geochemical and paleomagnetic results (Mahoney *et al.* 1993; Tejada *et al.* 1996; Neal *et al.* 1997; Antretter *et al.* 2003) make it appear less likely that the Louisville hotspot and Ontong-Java Plateau are genetically linked, allowing us to use a plume initiation age that is much younger than the ~122 Ma age of the Ontong Java Plateau. In this adjusted model, an even stronger (south)eastward motion is computed for the Louisville hotspot, leading to a somewhat faster relative motion between the plate and hotspot. As a result, the $^{40}Ar/^{39}Ar$ ages of the older parts of the Louisville and Hawaiian seamount trails (Sharp and Clague 2002; Tarduno *et al.* 2003) fit increasingly well (red continuous lines). This does not contradict the finding that the new age dates indicate a slower plate motion relative to the Louisville hotspot in the 80-62 Ma period, as we can achieve a good fit for that period by choosing a slower plate motion. Obviously, it may also be caused by a slower hotspot motion during that period, however, this does not occur in our numerical models. Using a younger plume initiation age is one way to achieve a better fit in these models, but there may be other ways as well. Due to the considerable spread of model results discussed below, the fact that an initiation age of 90 Ma yields a better fit than 120 Ma, does not comprise new evidence for disconnecting the formation of the Ontong Java Plateau from the Louisville hotspot.

The Louisville hotspot motion computed under different modeling assumptions may thus vary considerably. The average of a large number of model runs is a slow east- to southeastward motion over the last 90 Myr. In contrast to Hawaii, where the modeled hotspot motion essentially represents the straightening up of a conduit that had

been strongly tilted prior to 80 Ma, the Louisville hotspot motion approximately represents horizontal flow in the upper part of the lower mantle away from the subduction zones that are located to the west of the Louisville seamount trail (Figure 1). Contributions to this pattern are **(i)** a deep return flow opposite to Pacific plate motion, **(ii)** a flow outward from the upwelling "superplume" beneath the South Pacific that is towards the south in the vicinity of Louisville, and **(iii)** for some models, including the one used here, flow outward from a regional upwelling southeast of New Zealand that is towards the west in the vicinity of Louisville. The speed of computed hotspot motion varies among models, with some models yielding almost no hotspot motion, others somewhat more than 10 mm/yr. A more detailed discussion of the results for Louisville, and comparison with the results for Hawaii, is given by Antretter et al. (2003). Model Case 3 is meant to approximate the average of our new modeling results, but since this average motion is quite similar to Case 2, the predicted tracks (dark green lines) remain similar. Finally, we have replaced the Hawaiian hotspot motion by a simplified motion that has a slightly larger southward component (Case 4, orange line) to better match recent paleolatitude results for ODP Leg 197 (Tarduno *et al.* 2003).

In most of these model cases, the calculations show a good fit to the geometry of the seamount trails (left panels in Figure 6) and the changes in plate rotation around 25 and 47 Ma approximately correspond to the 159ºW and 169ºW bends in the Louisville seamount trail (Figure 1). This holds true for model Case 4, where the Hawaiian hotspot has moved southward between 83 and 47 Ma at a rate of approximately 35 mm/yr compatible with new paleolatitude data (Tarduno *et al.* 2003). In the same model, the Louisville hotspot has moved (south)eastward at a much slower rate, predicting a significant decrease in the distance between the two hotspots of about 1,000 km from 83 to 47 Ma. Despite this remarkable inter-hotspot motion, we can fit the observed geometries and the new $^{40}Ar/^{39}Ar$ age data in both seamount trails very well. For comparison, we also show the best fitting tracks and age progressions for fixed hotspots (Case 0, black lines). In the fixed hotspot case, the computed ages for the older part of the Hawaiian track tend to be too old by ~10 Ma, while its geometry is poorly fitted; the computed ages for the older part of the Louisville track are too young by ~5 Ma. We thus conclude that the fit seems better with moving hotspots than with fixed hotspots, which may seem surprising at first, since the combination of the Hawaiian and Louisville hotspot tracks was used previously to support the fixed hotspot hypothesis (e.g. Morgan 1972; Duncan and Richards 1991). However, this conclusion can be readily understood by considering how radiometric age dates have changed recently for the Hawaiian-Emperor and Louisville seamount trails. Ages for Detroit Seamount at the northern end of the Emperor seamount trail reported by Tarduno et al. (2003) are younger than previously determined (Keller *et al.* 1995), whereas the Hawaiian-Emperor bend now appears to be about 4 Myr older than previously assumed at 47 Ma (Sharp and Clague 2002). As a consequence, the motion of

the Pacific plate relative to the Hawaiian hotspot during the formation of the Emperor chain now appears significantly faster than previously understood. In contrast, based on the $^{40}Ar/^{39}Ar$ age dates reported in this paper, the motion of the Pacific plate relative to the Louisville hotspot during the same time interval now appears slower (Figure 2). While previous results supported the idea that the Hawaiian and Louisville hotspots are fixed relative to each other, the new results are better explained with a closing motion between the hotspots, particularly prior to 62 Ma. Based on this result, we expect that the difference between the ancient paleolatitudes of the Louisville seamount trail and the present day latitude of its hotspot is not as large as the difference between paleolatitudes of the Emperor seamount trail and the current location of the Hawaiian hotspot. We anticipate that it will be possible to confirm or refute this model prediction through future ocean drilling.

Finally, we consider plate motions and hotspot tracks globally (dotted and dashed grey lines) as in Steinberger et al. (2003). We can still obtain a good fit to both hotspot tracks and age progressions, but not quite as good as when considering the Pacific plate in isolation. The predicted curve for the Louisville age-distance plot is still close to the data points, but the slope of the older part is smaller than the slope inferred from the actual measured ages. The fit could be improved if we allow for variations of the motion of East *vs.* West Antarctica (within geological uncertainties) in the global plate circuit, instead of just using one particular case. This issue will be addressed in future work.

4. Summary

Based on major improvements in the $^{40}Ar/^{39}Ar$ dating technique over the last decades, we could successfully re-date 10 samples from the Watts et al. (1988) study by applying high-resolution incremental heating experiments. These improved ages show that the age progression for the Louisville seamount trail is ***not*** linear after all, given that samples from the old end of this seamount trail have incremental heating $^{40}Ar/^{39}Ar$ ages that are up to 18% older than the previous ages determined by the total fusion technique. This indicates that Pacific plate motion should have been slower prior to 62 Ma when compared to published plate rotation models. This also indicates that the age progression of the Louisville seamount trail ***cannot*** be explained by plate motion alone, but requires significant motion of the Louisville hotspot itself.

In this paper, we presented detailed mantle flow models (cf. Steinberger *et al.* 2003) to fit the geometries and age progressions of both the Hawaiian and Louisville hotspots. Our results indicate that the non-linear $^{40}Ar/^{39}Ar$ age progressions of the Hawaiian and Louisville hotspot tracks can be better modeled with a moving hotspot rather

than a fixed hotspot frame of reference. The same models also indicate that the primary Hawaiian and Louisville hotspots did not move in concert, showing significant inter-hotspot motion between 80 and 47 Ma. While the Hawaiian hotspot experienced a substantial ~15° southward motion prior to 47 Ma (Tarduno *et al.* 2003) based on paleolatitude data, the Louisville hotspot is predicted to have experienced an eastward motion of ~7º during the same geological period, followed by a minor ~2º latitudinal shift over the last 40 Myr.

Acknowledgments

We thank John Huard for technical support in the OSU argon dating laboratory. Financial support is provided by NSF-OCE 9730394 and NSF-OCE 0002875. Special thanks are for Hubert Staudigel, who kindly facilitated and encouraged the visits of AAPK to the OSU to perform the dating and to write this paper.

APPENDIX A
^{40}AR/^{39}AR ANALYTICAL DATA

All new $^{40}Ar/^{39}Ar$ age data reported in this study have been calculated using ArArCALC v2.2 (Koppers 2002) and their resulting *.AGE files have been included in this electronic appendix. The same files also have been saved in the standard Microsoft Excel format (with the *.XLS extension) and can be opened without running ArArCALC. In the table below each high-resolution incremental heating experiment is listed together with their filenames and an URL to download these files from the EarthRef Digital Archive (ERDA):

Sample Number	Sample Type	Archive Name	ERDA Hyperlink
SOTW-9-58-1a	Groundmass	01C2259.zip	http://earthref.org/cgi-bin/erda.cgi?n=193
SOTW-9-58-7	Groundmass	01C1919.zip	http://earthref.org/cgi-bin/erda.cgi?n=194
SOTW-9-52-1	Groundmass	03C3173.zip	http://earthref.org/cgi-bin/erda.cgi?n=195
SOTW-9-48-2	Groundmass	03C3213.zip	http://earthref.org/cgi-bin/erda.cgi?n=196
VM36-04	Groundmass	03C3112.zip	http://earthref.org/cgi-bin/erda.cgi?n=197
VM36-03	Groundmass Plagioclase	03C3145.03C3276.03C3258.zip	http://earthref.org/cgi-bin/erda.cgi?n=198
VM36-02	Groundmass	03C3309.03C3080.zip	http://earthref.org/cgi-bin/erda.cgi?n=199
VG-3a/MSN110-1	Groundmass	01C2051.zip	http://earthref.org/cgi-bin/erda.cgi?n=200
MTHN-6D1	Groundmass	01C2177.zip	http://earthref.org/cgi-bin/erda.cgi?n=201
MTHN-7D1	Groundmass	01C2027.zip	http://earthref.org/cgi-bin/erda.cgi?n=202

Note that all electronic data supplements that are related to this publication can be listed online EarthRef by selecting the http://earthref.org/cgi-bin/err.cgi?n=5002 link and by following the Quick Links. The ArArCALC v2.2 software can be directly downloaded via the http://earthref.org/cgi-bin/erda.cgi?n=133 link, whereas the ArArCALIBRATIONS tool can be retrieved from http://earthref.org/cgi-bin/erda.cgi?n=139.

FIGURE CAPTIONS

Figure 1. Location map of the Louisville seamount trail after Lonsdale (1988). The seafloor magnetic anomalies (Cande and Kent 1995), some important morphological features and the fracture zones in the underlying oceanic basement are shown for reference. Two changes in orientation (bends) can be recognized in this seamount trail at 169ºW and 159ºW close to where it intersects with the Wishbone Scarp and Tharp fracture zone. Filled circles are guyots, whereas the plus signs indicate seamounts. Re-dated guyots are indicated by red circles. Note that the youngest dated sample MTHN-7D1 falls of this map and is located at 50º26'S and 139º09'W.

Figure 2. Comparison of new incremental heating $^{40}Ar/^{39}Ar$ ages with total fusion ages after Watts et al. (1988). The new ages are up to 11-12 Myr older in the oldest part of the Louisville seamount trail (Table 3). Samples younger than 62 Myr are more compatible with previous total fusion ages, although the analytical precision in these age determinations is significantly improved (Table 3). The new incremental heating dates thus show a non-linear age progression as indicated by the orange dashed line, which follows the oldest observed ages. An alternate age progression is shown by the purple dotted line as based on mantle convection models of Steinberger et al. (2003). Their models allow for the movement of the Louisville hotspot over geological time, which is reflected in a different age-distance relationship that is consistent with the older ages for Osbourn seamount, but not with the general age trend. Improved models show a better agreement, as displayed in Figure 6.

Figure 3. High-resolution incremental heating $^{40}Ar/^{39}Ar$ analyses for Louisville seamount trail basalts. The reported $^{40}Ar/^{39}Ar$ ages are weighted age estimates with errors reported on the 95% confidence level, including 0.3-0.4% standard deviations in the J-value. All samples where monitored against FCT-3 biotite (28.04 ± 0.18 Ma, 1σ) as calibrated by Renne et al. (1998). Data are listed in Table 2 and ArArCALC age calculation files can be downloaded from the Table in Appendix A.

Figure 4. Three examples of typical degassing behavior in the groundmass $^{40}Ar/^{39}Ar$ analyses. In this representation, we display for each increment the fraction of the $^{36}Ar_{atm}$ and $^{37}Ar_{ca}$ and $^{38}Ar_{cl}$ components relative to the total amount of gas released during the experiment. These percentages have been normalized to the size of each degassing step, as approximated by the size of the $^{39}Ar_k$ component. Clear spikes are visible at the beginning and the end of each degassing spectra, reflecting the degassing of alteration products at low temperatures and high-Ca minerals, such as plagioclase and clinopyroxene, at high temperatures.

Figure 5. Schematic isochron diagram explaining the low and high temperature deviations routinely observed in groundmass $^{40}Ar/^{39}Ar$ analyses as caused by submarine alteration. This diagram shows that disturbances due to alteration can be resolved by performing high-resolution incremental heating experiments (15-30 increments) on groundmasses that have been cleaned with an enhanced acid-leaching procedure. After Koppers et al. (2000).

Figure 6. Mantle flow modeling results. Computed hotspot motion and tracks **(A)** and age-distance plots **(B)** for the Hawaiian and Louisville hotspots. Hotspot motion during the past 120 Ma is shown as rainbow-colored lines for Case 2 only (see below) as indicated by the colored scale bar; tracks and age-distance relation are shown as

single-colored lines for all cases discussed. Tickmark intervals are 10 Ma. Results are shown for the following models: Case [0] – black lines: fixed hotspots; best-fitting Pacific plate motion with four different rotations 0-25 Ma, 25-43 Ma, 43-62 Ma, 62-83 Ma and an assumed plume initiation age of 120 Ma for the Louisville hotspot. Case [1] – brown lines: Hotspot motion as in Steinberger et al. (2003) with the same time intervals and plume initiation ages as in case 0. Case [2] – red lines: Hotspot motion (shown here) computed for assumed initiation age 90 Ma for Louisville plume; other model assumptions are the same as in Case 1. For this case, three different plate motion models are considered: Case [2A] – continuous line: best-fitting Pacific plate motion with time intervals as in case 0. Case [2B] – dashed grey line: best fit to hotspot tracks on both hemispheres, with global plate circuit model 3 of Steinberger et al. (2003); four rotations of African plate with time intervals as in Case 0. Case [2C] – dotted grey line: three rotations of African plate for time intervals 0-43 Ma, 43-62 Ma, 62-83 Ma; otherwise as Case 2B. Case [3] – dark green lines: Louisville hotspot moved 7 degrees eastward and 2 degrees southward during past 120 Ma at constant speed; otherwise as case 1. Case [4] – orange line: Hawaiian hotspot moved, at constant speed, 2 degrees eastward and 2 degrees southward during past 47 Ma, and 3 degrees eastward and 13 degrees southward between 90 and 47 Ma; otherwise as Case 3.

TABLE CAPTIONS

Table 1.
Sample locations in the Louisville seamount trail.

[Caption with Table 1.]
No caption.

Table 2.
Incremental heating $^{40}Ar/^{39}Ar$ analyses on Louisville seamount basalts.

[Caption with Table 2.]
K/Ca values are calculated as weighted means for the age spectra or using recombined totals of $^{39}Ar_K$ and $^{37}Ar_{Ca}$ for the total fusions. MSWD values for the age plateaus and inverse isochrons are calculated using N-1 and N-2 degrees of freedom, respectively. All samples from this study where monitored against FCT-3 biotite (28.04 ± 0.18 Ma) as calibrated by Renne et al. (1998). Reported errors on the $^{40}Ar/^{39}Ar$ ages are on the 95% confidence level including 0.3-0.4% standard deviation in the J-value. All input parameters to the calculations are published in Table 2 of Koppers et al. (2003a).

Table 3.
Comparison of $^{40}Ar/^{39}Ar$ total fusion and high-resolution incremental heating ages.

[Caption with Table 3.]
The difference in age is most prominent for Osbourn seamount with an 16% increase, whereas the youngest sample dated has been more than doubled in age when compared to the total fusion age. The precision has increased for all samples by showing 10-89% improvements. Note that Watts et al. (1988) used MMhb-1 calibrated by Dalrymple et al. (1981) at 519.5 ± 2.5 Ma (1σ) to calibrate its internal $^{40}Ar/^{39}Ar$ ages, whereas this study uses FCT-3 at 28.04 ± 0.18 Ma (Renne *et al.* 1998). To make age comparisons possible, we used the ArArCALIBRATIONS tool (Appendix A) to recalibrate the Watts et al. (1988) ages towards the FCT-3 standard based on the explicit age equations of Min et al. (2000) as detailed in Koppers (2002).

REFERENCES

Antretter, M, Riisager, P, Hall, S, Zhao, X and Steinberger, B (2003). Modeled paleolatitudes for the Louisville hotspot and the Ontong Java Plateau. In: *Origin and Evolution of the Ontong Java Plateau. G Fitton, J Mahoney, P Wallace and A Saunders. London, The Geological Society, London, U. K. In Revision*.

Cande, SC and Kent, DV (1995). Revised Calibration of the Geomagnetic Polarity Timescale for the Late Cretaceous and Cenozoic. *Journal of Geophysical Research-Solid Earth 100(B4): 6093-6095*.

Courtillot, V, Davaille, A, Besse, J and Stock, J (2003). Three distinct types of hotspots in the Earth's mantle. *Earth and Planetary Science Letters 205(3-4): 295-308*.

Dalrymple, GB, Alexander, EC, Lanphere, MA and Kraker, GP (1981). Irradiation of samples for 40Ar/39Ar dating using the Geological Survey TRIGA reactor. *U.S. Geological Survey, Proffesional Paper 1176: 55*.

Duncan, RA and Clague, DA (1985). Pacific plate motion recorded by linear volcanic chains. In: *The ocean basins and margins. AEA Nairn, FL Stehli and S Uyeda. New York, Plenum Press. 7A: The Pacific ocean: 89-121*.

Duncan, RA and Richards, MA (1991). Hotspots, mantle plumes, flood basalts, and true polar wander. *Reviews of Geophysics 29: 31-50*.

Foulger, GR and Natland, JH (2003). Is "hotspot" volcanism a consequence of plate tectonics? *Science 300(5621): 921-922*.

Hawkins, JW, Lonsdale, PF and Batiza, R (1987). Petrologic evolution of the Louisville seamount chain. In: *American Geophysical Union Monograph. BH Keating, P Fryer, R Batiza and GW Boehlert. 43: 235-254*.

Keller, RA, Duncan, RA and Fisk, MR, Eds. (1995). Geochemistry and 40Ar/39Ar geochronology of basalts from ODP Leg 145.

Koppers, AAP (2002). ArArCALC - software for Ar-40/Ar-39 age calculations. *Computers & Geosciences 28(5): 605-619*.

Koppers, AAP, Morgan, JP, Morgan, JW and Staudigel, H (2001). Testing the fixed hotspot hypothesis using Ar-40/Ar-39 age progressions along seamount trails. *Earth and Planetary Science Letters 185(3-4): 237-252*.

Koppers, AAP, Staudigel, H and Duncan, RA (2003a). High-resolution $^{40}Ar/^{39}Ar$ dating of the oldest oceanic basement basalts in the western Pacific basin. *Geochemistry Geophysics Geosystems 4: In Press*.

Koppers, AAP, Staudigel, H and Wijbrans, JR (2000). Dating crystalline groundmass separates of altered Cretaceous seamount basalts by the Ar-40/Ar-39 incremental heating technique. *Chemical Geology 166(1-2): 139-158*.

Koppers, AAP, Staudigel, H, Wijbrans, JR and Pringle, MS (1998). The Magellan seamount trail: implications for Cretaceous hotspot volcanism and absolute Pacific plate motion. *Earth and Planetary Science Letters 163(1-4): 53-68*.

Koppers, AAP, Staudigel, H, Wijbrans, JR and Pringle, MS (2003b). Short-lived and discontinuous intraplate volcanism in the South Pacific: hot spots or extensional volcanism? *Geochemistry Geophysics Geosystems 4: -*.

Kuiper, YD (2002). The interpretation of inverse isochron diagrams in Ar-40/Ar-39 geochronology. *Earth and Planetary Science Letters 203(1): 499-506*.

Lonsdale, P (1988). Geography and history of the Louisville hotspot chain in the Southwest Pacific. *Journal of Geophysical Research 93: 3,078-3,104*.

Mahoney, JJ, Storey, M, Duncan, RA, Spencer, KJ and Pringle, MS (1993). Geochemistry and Age of the Ontong Java Plateau. In: *The Mesozoic Pacific: geology, tectonics, and volcanism. MS Pringle, WW Sager, WV Sliter and S Stein. Washington, D.C., Am. Geophys. Un. 77 (Schlanger Volume): 233-261*.

McDougall, I and Harrison, TM (1988). Geochronology and thermochronology by the $^{40}Ar/^{39}Ar$ method. *Oxford University Press. 212 pages.*

Min, KW, Mundil, R, Renne, PR and Ludwig, KR (2000). A test for systematic errors in Ar-40/Ar-39 geochronology through comparison with U/Pb analysis of a 1.1-Ga rhyolite. *Geochimica Et Cosmochimica Acta 64(1): 73-98*.

Morgan, WJ (1972). Plate motions and deep mantle convection. *Geological Society of America Memoir 132 (Hess Volume): 7-122*.

Neal, CR, Mahoney, JJ, Kroenke, LW, Duncan, RA and Petterson, MG (1997). The Ontong Java Plateau. In: *Large Igneous Provinces: Continental, Oceanic, and Planetary Flood Volcanism. JJ Mahoney and M Coffin. 100: 183-216*.

Renne, PR, Deino, AL, Walter, RC, Turrin, BD, Swisher III, CC, Becker, TA, Curtis, GH, Sharp, WD and Jaouni, A-R (1994). Intercalibration of astronomical and radioisotopic time. *Geology 22: 783-786*.

Renne, PR, Swisher, CC, Deino, AL, Karner, DB, Owens, TL and DePaolo, DJ (1998). Intercalibration of standards, absolute ages and uncertainties in $^{40}Ar/^{39}Ar$ dating. *Chemical Geology 145: 117-152*.

Sharp, WD and Clague, DA (2002). An Older, Slower Hawaii-Emperor Bend. *Eos Trans. AGU 83(47): Abstract T61C-04*.

Smith, AD and Lewis, C (1999). Differential rotation of lithosphere and mantle and the driving forces of plate tectonics. *Journal of Geodynamics 28(2-3): 97-116*.

Steiger, RH and Jager, E (1977). Subcommission on geochronology: convention on the use of decay constants in geo- and cosmochronology. *Earth and Planetary Science Letters 36: 359-362*.

Steinberger, B (2000). Plumes in a convecting mantle: Models and observations for individual hotspots. *Journal of Geophysical Research-Solid Earth 105(B5): 11127-11152*.

Steinberger, B and O'Connell, RJ (1998). Advection of plumes in mantle flow: implications for hotspot motion, mantle viscosity and plume distribution. *Geophysical Journal International 132(2): 412-434*.

Steinberger, B, Sutherland, R and O'Connell, RJ (2003). Mantle flow models constrained by revised global plate motions successfully predict the Emperor-Hawaii and other hotspot-related seamount chains. *Nature: Submitted*.

Tarduno, JA, Duncan, RA, Scholl, DW, Cottrell, RD, Steinberger, B, Thordarson, T, Kerr, BC, Neal, CR, Frey, FA, Torii, M and Carvallo, C (2003). The Emperor Seamounts: Southward motion of the Hawaiian hotspot plume in Earth's mantle. *Science 301: 1,064-1,069*.

Taylor, JR (1997). An introduction to error analysis. *Mill Valley, California, University Science Books. 327 pages.*

Tejada, MLG, Mahoney, JJ, Duncan, RA and Hawkins, MP (1996). Age and geochemistry of basement and alkalic rocks of Malaita and Santa Isabel, Solomon Islands, southern margin of Ontong Java plateau. *Journal of Petrology 37(2): 361-394*.

Watts, AB, Weissel, JK, Duncan, RA and Larson, RL (1988). Origin of the Louisville Ridge and its relationship to the Eltanin fracture zone system. *Journal of Geophysical Research 93: 3,051-3,077*.

Wessel, P and Kroenke, L (1997). A geometric technique for relocating hotspots and refining absolute plate motions. *Nature 387: 365-369*.

York, D (1969). Least squares fitting of a straight line with correlated errors. *Earth and Planetary Science Letters 5: 320-324*.

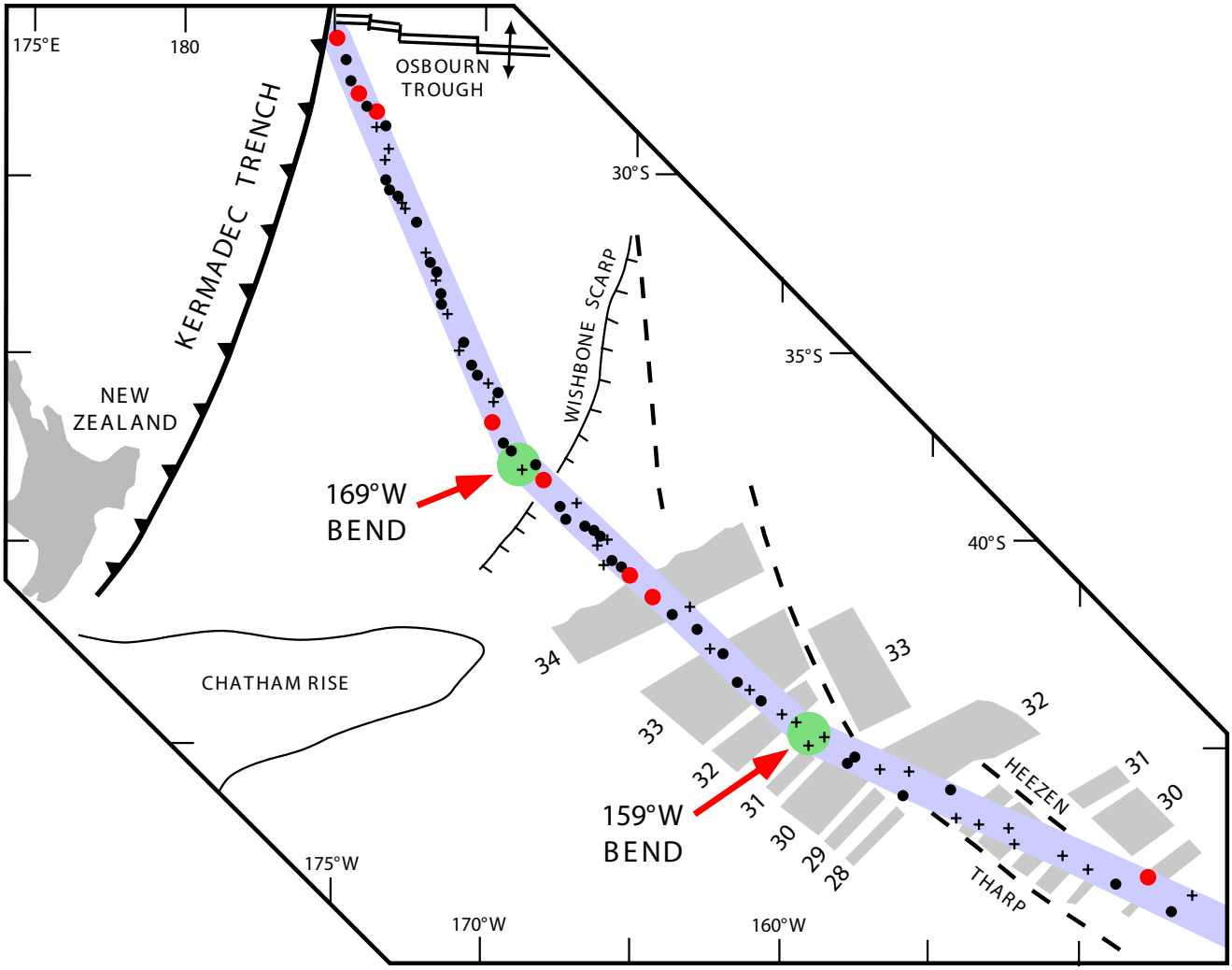

Figure 1
Koppers et al. 2003

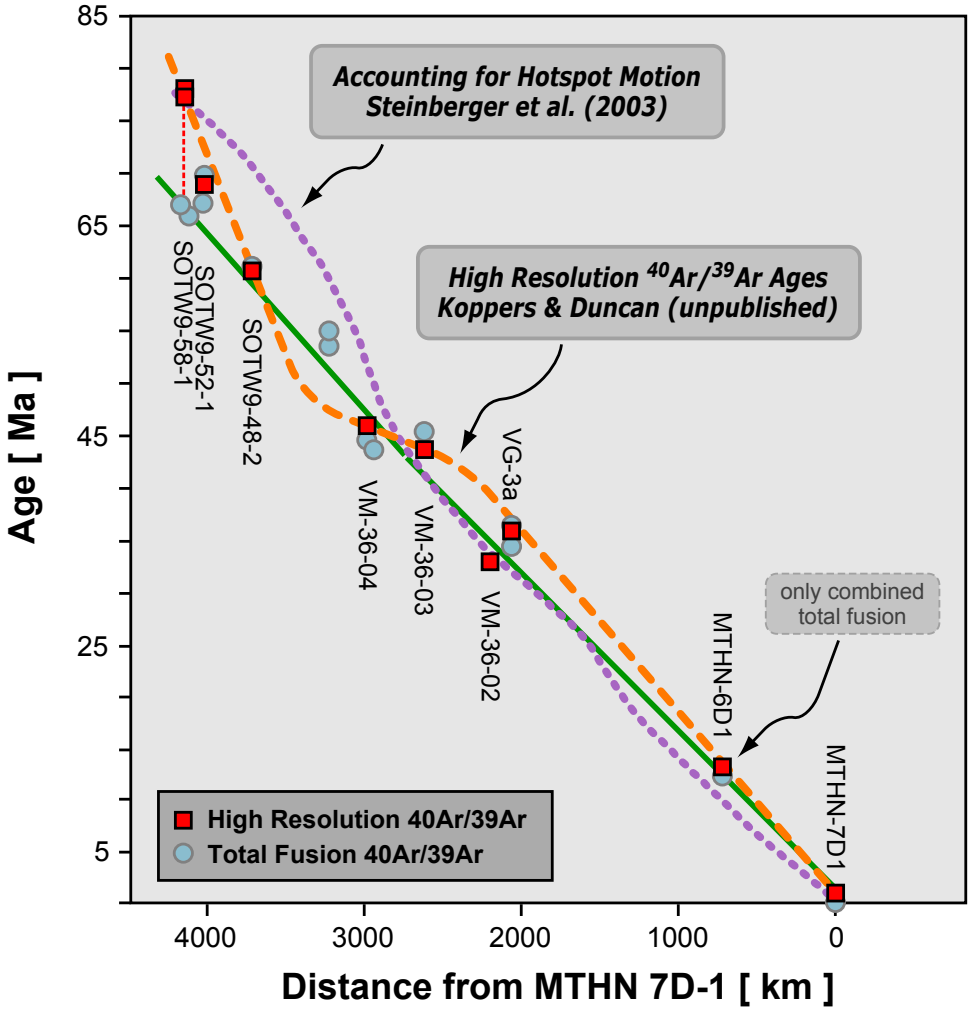

Figure 2
Koppers et al. 2003

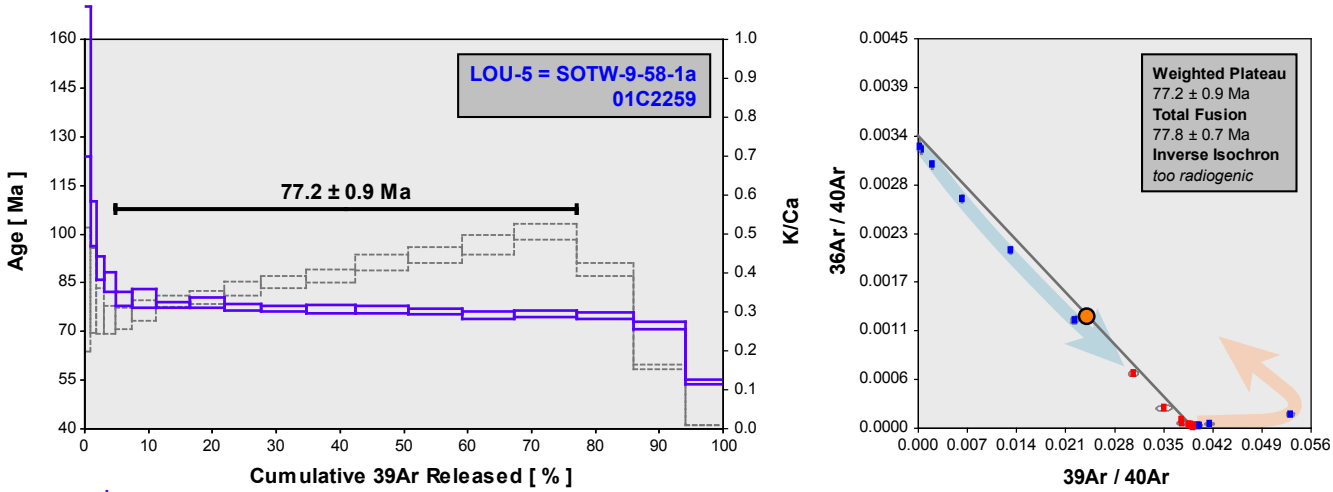

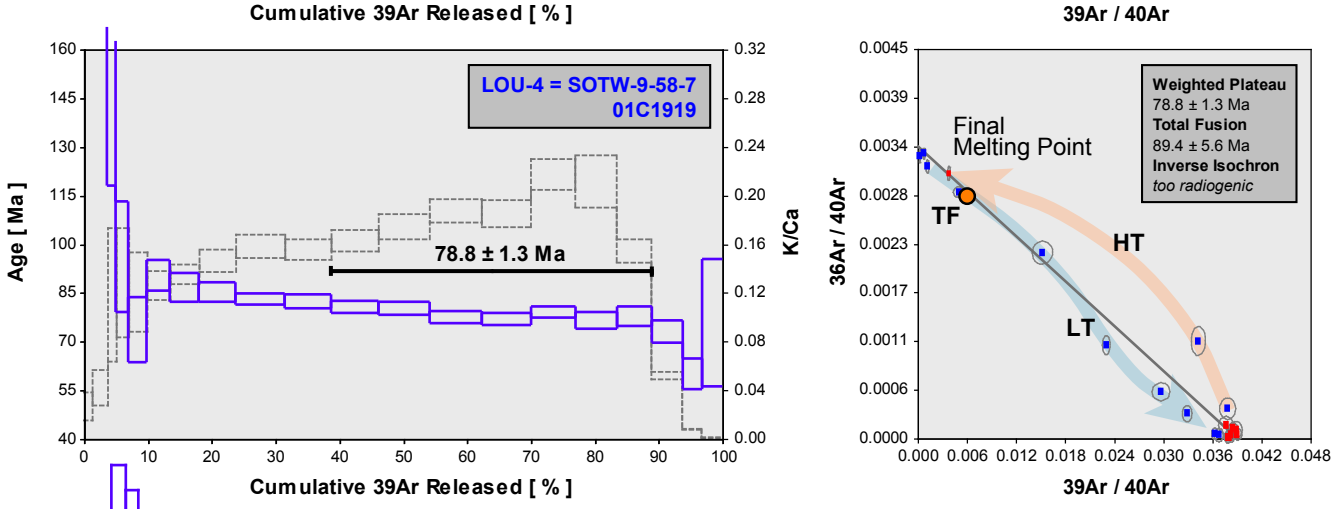

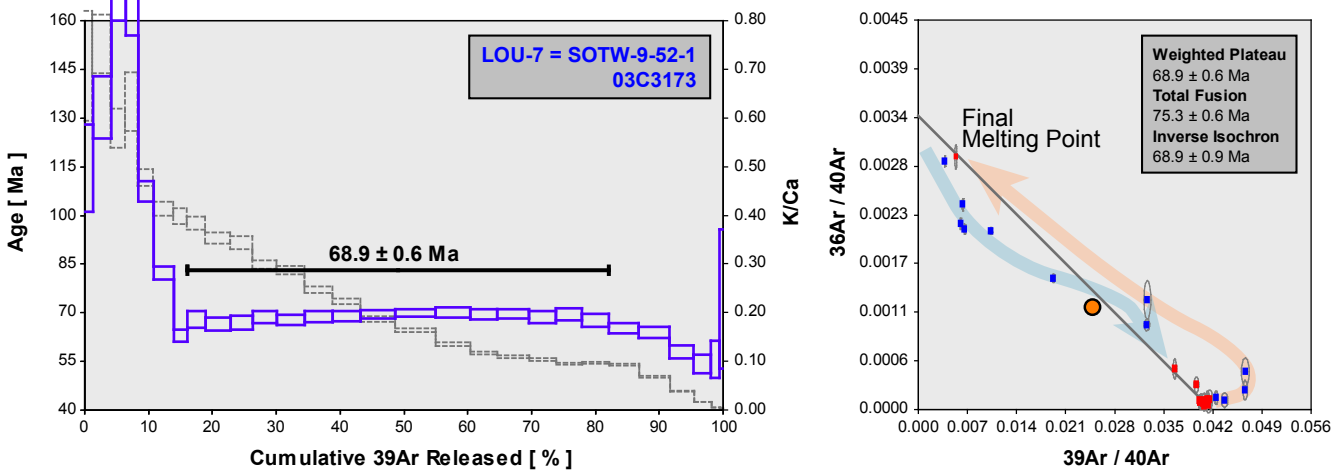

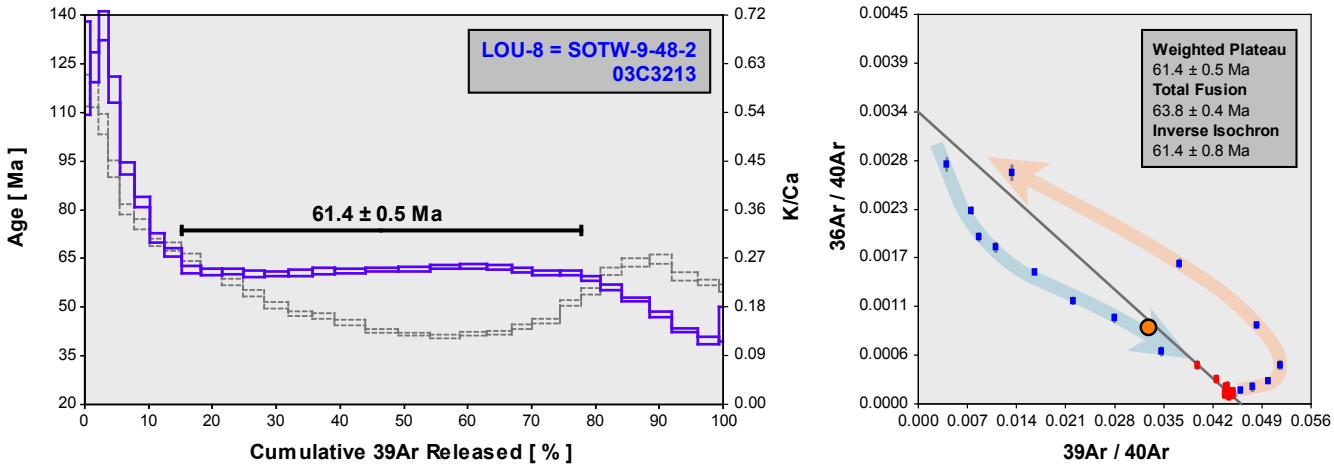

Figure 3a
Koppers et al. 2003

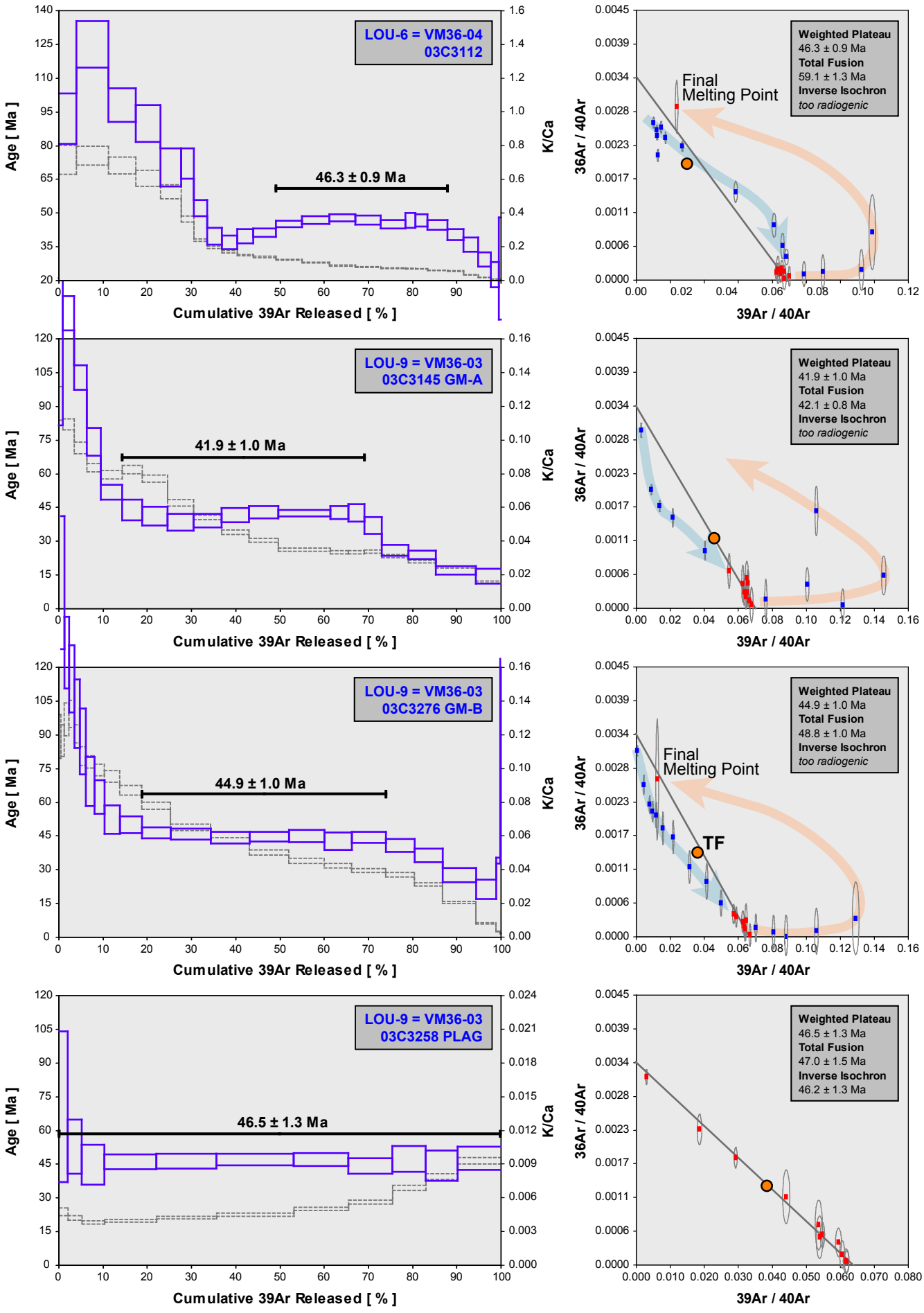

Figure 3b
Koppers et al. 2003

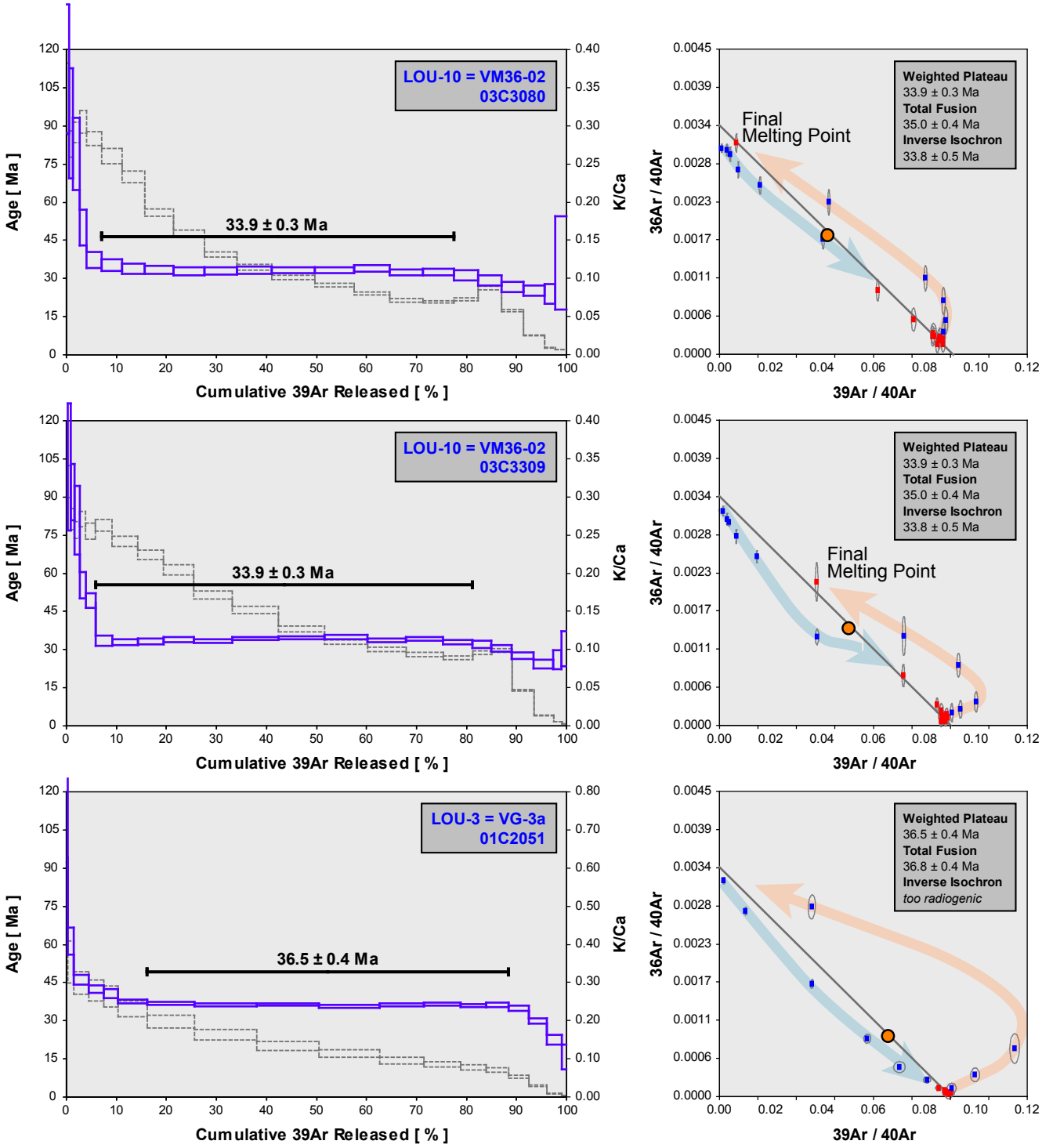

Figure 3c
Koppers et al. 2003

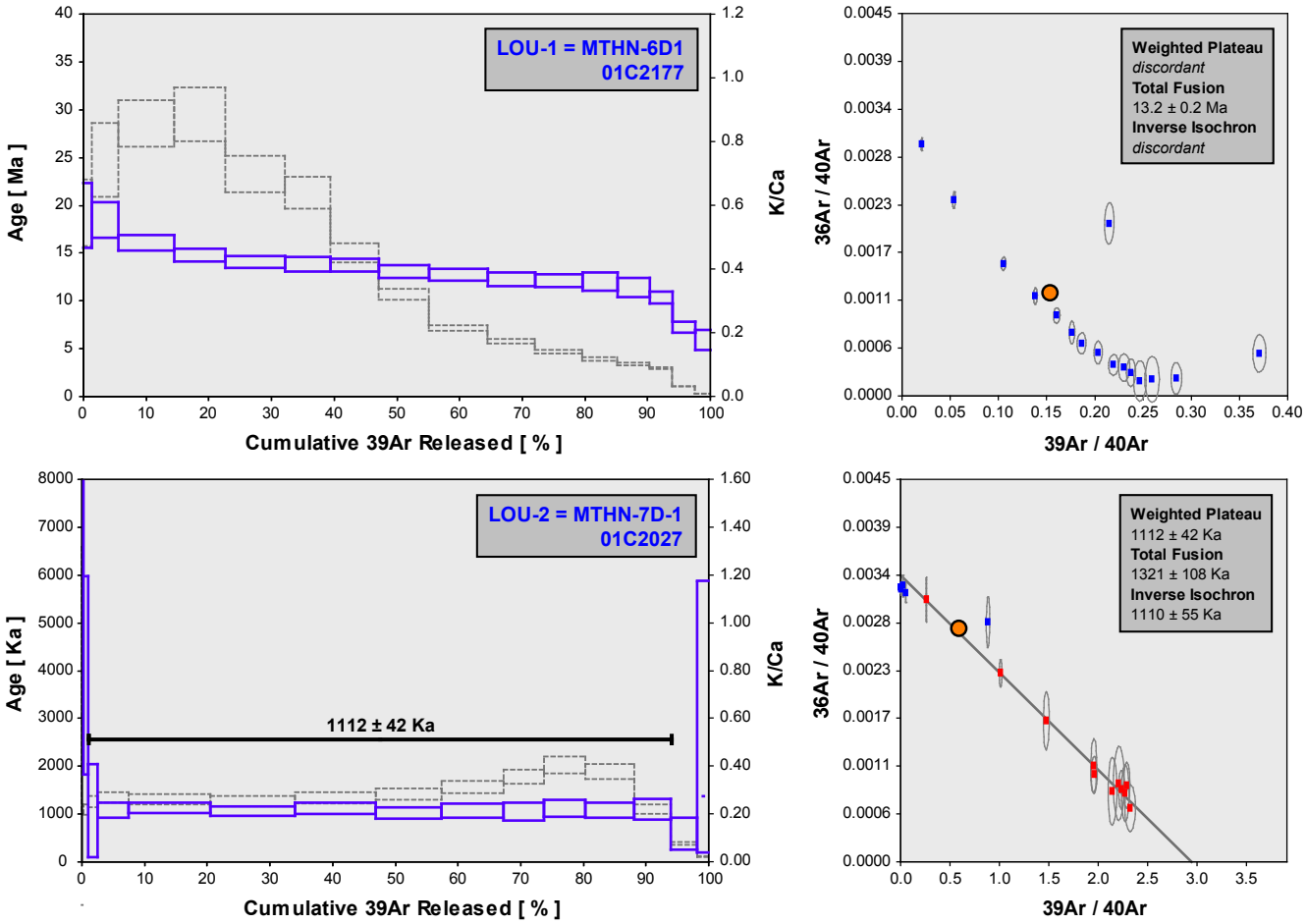

Figure 3d
Koppers et al. 2003

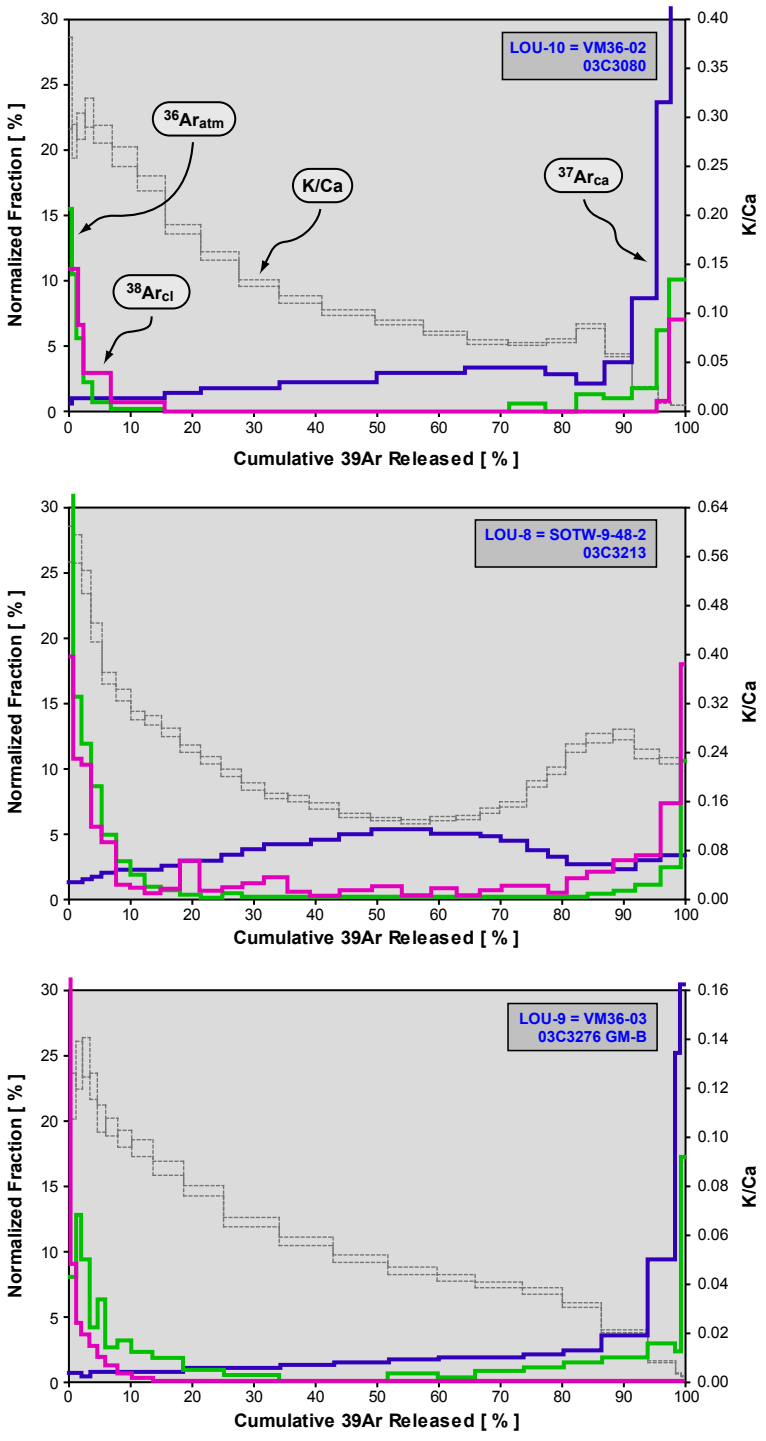

Figure 4
Koppers et al. 2003

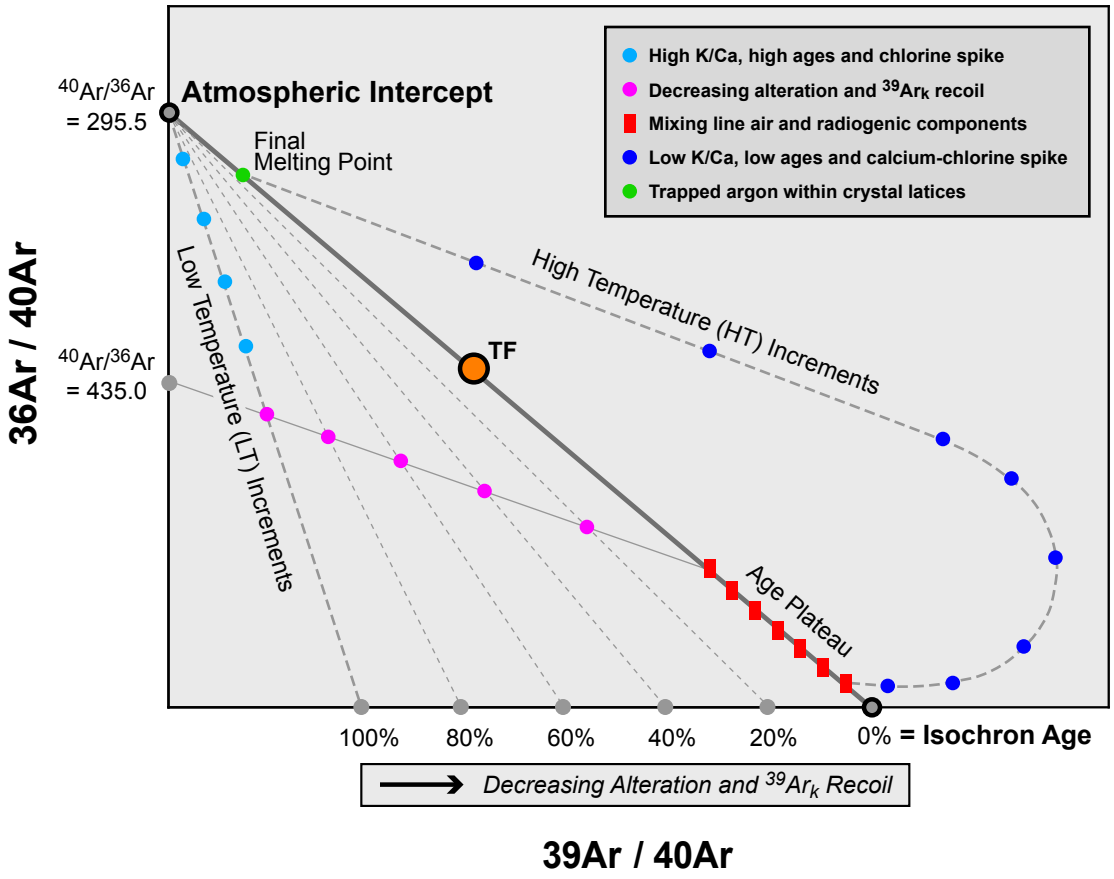

Figure 5
Koppers et al. 2003

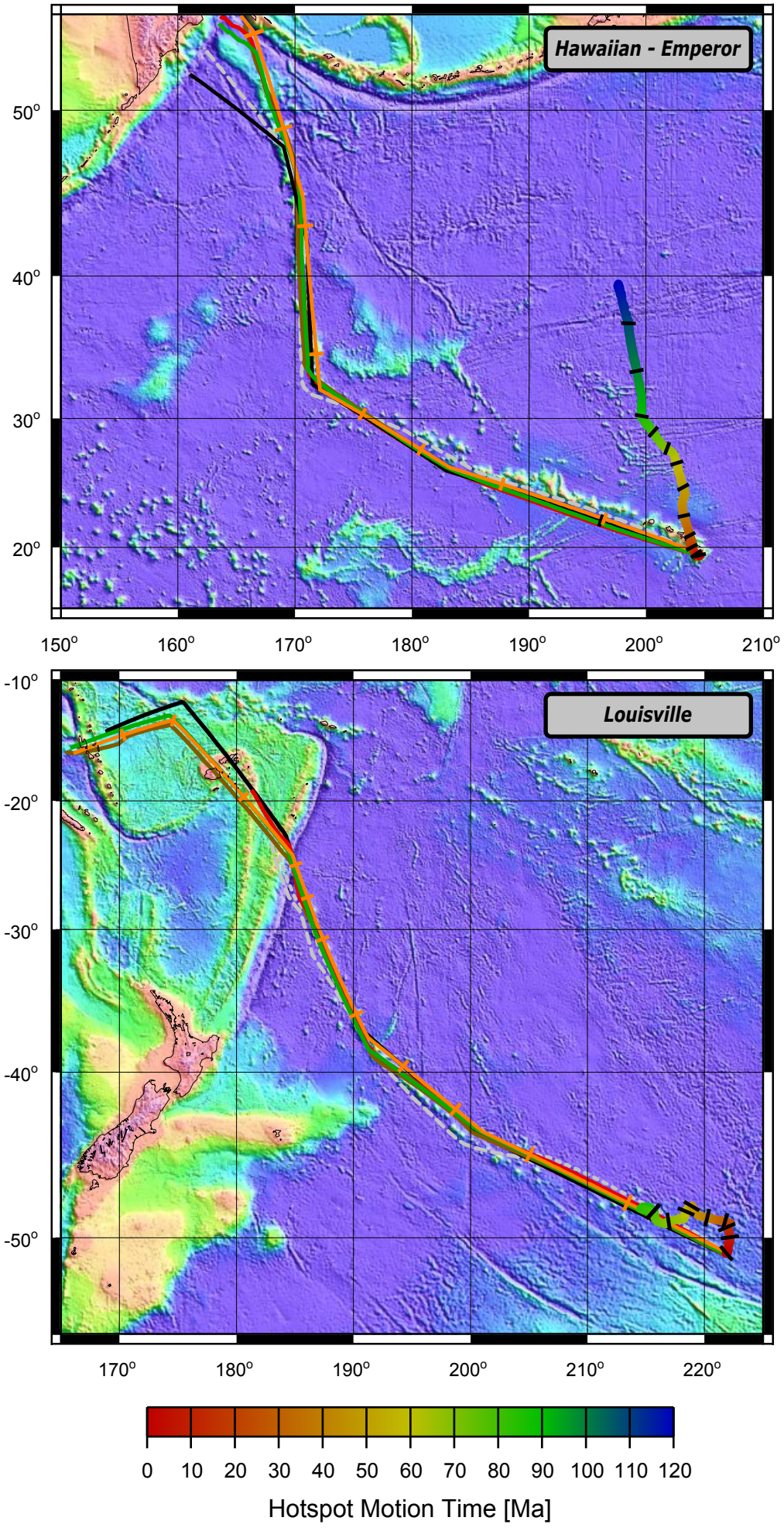

Figure 6a
Koppers et al. 2003

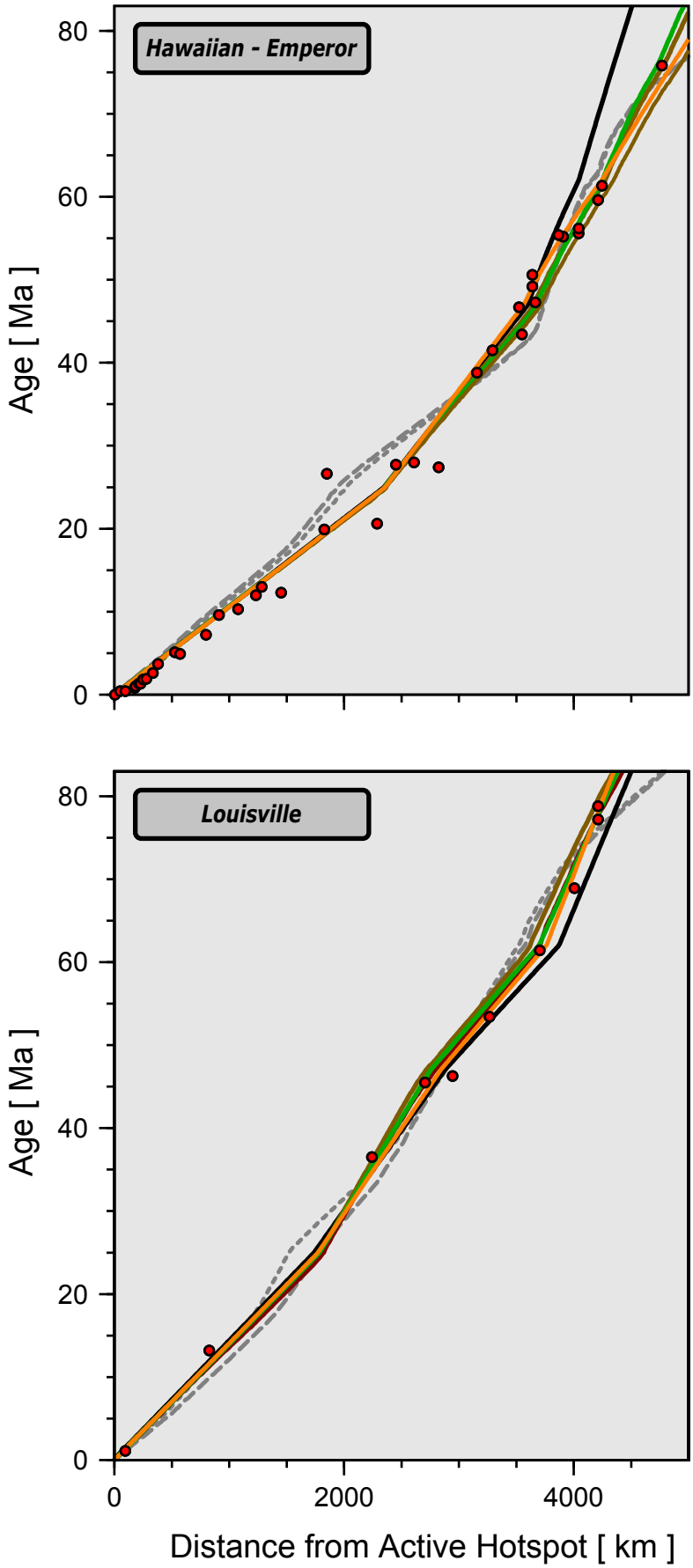

Figure 6b
Koppers et al. 2003

Louisville Seamount Trail Argon Geochronology
Koppers et al. 2003

Sample Number	Seamount Name	Lat	Lon	Distance (km)	Depth (mbsl)	Rock Type	Cruise Name
Northwestern Segment							
SOTW-9-58-1a	Osbourn	25º31.8'S	174º02.4'W	4060	2443	Basanite	SOUTHTOW09-1972
SOTW-9-58-7	Osbourn	25º31.8'S	174º02.4'W	4060	2443	Olivine Nephelenite	SOUTHTOW09-1972
SOTW-9-52-1		27º16.8'S	174º12.6'W	3919	3480	Hawaiite	SOUTHTOW09-1972
SOTW-9-48-2	Currituck	30º06.0'S	173º15.0'W	3625	2300	Hawaiite	SOUTHTOW09-1972
VM36-05		33º56.7'S	171º11.5'W	3175	2760	Alkali Basalt	VEMA36-02-1979
Middle Segment							
VM36-04		36º57.0'S	169º50.0'W	2856	1446	Picritic Basalt	VEMA36-02-1979
VM36-03		38º19.5'S	167º43.7'W	2616	1232	Alkali Basalt	VEMA36-02-1979
VM36-02		40º47.0'S	165º21.0'W	2286	1883	Alkali Basalt	VEMA36-01-1979
VG-3a/MSN110-1	Valerie	41º36.8'S	164º12.0'W	2154	950	Alkali Basalt	MONSOON07-1961
Southeastern Segment							
MTHN-6D1		48º12.0'S	148º48.0'W	742	720	Alkali Basalt	MARATHON06-1984
MTHN-7D1		50º26.0'S	139º09.0'W	0	640	Alkali Basalt	MARATHON06-1984

Sample Number	Lab Code	Experiment Number	Sample Type		Age Spectrum Age ± 2σ (Ma)	^{39}Ar (%)	K/Ca	MSWD	n	Total Fusion Age ± 2σ (Ma)	Inverse Isochron Analyses Age ± 2σ (Ma)	^{40}Ar/ ^{36}Ar intercept	MSWD
Northwestern Segment													
SOTW-9-58-1a	LOU-5	01C2259	Groundmass		77.2 ± 0.9	72	0.381	5.3	11	77.8 ± 0.7			
SOTW-9-58-7	LOU-4	01C1919	Groundmass		78.8 ± 1.3	50	0.179	2.4	7	89.4 ± 5.6			
SOTW-9-52-1	LOU-7	03C3173	Groundmass		68.9 ± 0.6	67	0.132	1.5	15	75.3 ± 0.6	68.9 ± 0.9	294.8 ± 110	1.7
SOTW-9-48-2	LOU-8	03C3213	Groundmass		61.4 ± 0.5	63	0.154	3.8	16	63.8 ± 0.4	61.4 ± 0.8	298.9 ± 81.7	4.1
Middle Segment													
VM36-04	LOU-6	03C3112	Groundmass		46.3 ± 0.9	39	0.072	1.6	8	59.1 ± 1.3			
VM36-03	LOU-9	03C3145	Groundmass	A	41.9 ± 1.0	55	0.042	1.2	9	42.1 ± 0.8			
		03C3276	Groundmass	B	44.9 ± 1.0	55	0.050	0.7	7	48.8 ± 1.0			
		03C3258	Plagioclase	C	46.5 ± 1.3	100	0.005	0.6	11	47.0 ± 1.5	46.2 ± 1.3	304.5 ± 10.8	0.4
			Combined	A+B+C	44.0 ± 0.9			2.3	27	45.5 ± 0.6	43.8 ± 0.9	311.4 ± 15.5	2.0
			Combined	B+C	45.5 ± 0.8			0.8	18	47.8 ± 0.9	45.3 ± 0.8	306.6 ± 10.8	0.6
VM36-02	LOU-10	03C3309	Groundmass	A	34.1 ± 0.4	75	0.123	2.8	11	35.3 ± 0.4	34.1 ± 0.6	294.0 ± 129	3.1
		03C3080	Groundmass	B	33.2 ± 0.4	70	0.094	0.9	11	34.7 ± 0.7	32.6 ± 0.8	357.1 ± 68.8	0.5
			Combined	A+B	33.9 ± 0.3	73	0.105	2.4	22	35.0 ± 0.4	33.8 ± 0.5	314.0 ± 68.9	2.5
VG-3a/MSN110-1	LOU-3	01C2051	Groundmass		36.5 ± 0.4	72	0.094	1.5	8	36.8 ± 0.4			
Southeastern Segment													
MTHN-6D1	LOU-1	01C2177	Groundmass							13.2 ± 0.2			
MTHN-7D1	LOU-2	01C2027	Groundmass		1.112 ± 0.042	93	0.275	0.3	11	1.321 ± 0.108	1.110 ± 0.055	296.9 ± 18.7	0.4

		This Study (2003)		Watts et al. (1988)		Differences	
Sample Number	Lab Code	Age ± 2σ (Ma)	n	Age ± 2σ (Ma)	Repeat (Ma)	Age (%)	Error (%)
Northwestern Segment							
SOTW-9-58-1a	LOU-5	77.2 ± 0.9	1	66.6 ± 1.2	65.9 ± 1.2	16%	-25%
SOTW-9-58-7	LOU-4	78.8 ± 1.3	1				
SOTW-9-52-1	LOU-7	68.9 ± 0.6	1	66.7 ± 2.8	70.1 ± 2.8	3%	-79%
SOTW-9-48-2	LOU-8	61.4 ± 0.5	1	61.2 ± 1.8		0%	-72%
VM36-05				53.4 ± 5.2			
Middle Segment							
VM36-04	LOU-6	46.3 ± 0.9	1	44.6 ± 1.0		4%	-10%
VM36-03	LOU-9	45.5 ± 0.8	3	45.5 ± 1.0		0%	-20%
VM36-02	LOU-10	33.9 ± 0.3	2				
VG-3a/MSN110-1	LOU-3	36.5 ± 0.4	1	36.6 ± 1.2	34.4 ± 1.2	0%	-67%
Southeastern Segment							
MTHN-6D1	LOU-1	13.2 ± 0.2	1	12.5 ± 0.8		6%	-75%
MTHN-7D1	LOU-2	1.112 ± 0.042	1	0.5 ± 0.4		122%	-89%